

# Characterizing the spin state of an atomic ensemble using the magneto-optical resonance method.

B. Julsgaard, J. Sherson, J. L. Sørensen  
*QUANTOP - Danish Quantum Optics Center*  
*Institute of Physics and Astronomy,*  
*University of Aarhus, 8000 Aarhus, Denmark*

E. S. Polzik\*  
*QUANTOP - Danish Quantum Optics Center*  
*Niels Bohr Institute, 2100 Copenhagen Ø, Denmark*  
(Dated: November 5, 2018)

Quantum information protocols utilizing atomic ensembles require preparation of a coherent spin state (CSS) of the ensemble as an important starting point. We investigate the magneto-optical resonance method for characterizing a spin state of cesium atoms in a paraffin coated vapor cell. Atoms in a constant magnetic field are subject to an off-resonant laser beam and an RF magnetic field. The spectrum of the Zeeman sub-levels, in particular the weak quadratic Zeeman effect, enables us to measure the spin orientation, the number of atoms, and the transverse spin coherence time. Notably the use of 894nm pumping light on the  $D1$ -line, ensuring the state  $F = 4$ ,  $m_F = 4$  to be a dark state, helps us to achieve spin orientation of better than 98%. Hence we can establish a CSS with high accuracy which is critical for the analysis of the entangled states of atoms.

PACS numbers: 32.30.Dx, 32.80.Bx, 76.70.Hb

## I. INTRODUCTION

The spin state of ensembles of alkaline atoms have been studied for a long time in many different contexts, e.g. sensitive magnetic field measurements [1], frequency standards [2], and recently within the field of quantum information. Coherent transfer of states of the electromagnetic field to atomic spin states with the aid of electromagnetically induced transparency has been demonstrated [3, 4]. A sample of cesium atoms has been spin squeezed [5], two samples of cesium atoms have been entangled [6], and in [7, 8] the sensitivity of atomic spin states to quantum fluctuations of the electromagnetic field was demonstrated. Some of these experiments require the preparation of a coherent spin state, CSS, (e.g. all atoms pumped into the magnetic substate  $F = 4$ ,  $m_F = 4$  in the cesium ground state).

This paper provides a detailed report on the creation and characterization of the coherent spin state used in the recent experiments on entanglement and quantum memory [6, 7, 8]. The importance of the CSS of a macroscopic ensemble is primarily in that the transverse spin components of this state are in the minimum uncertainty state and thus provide a necessary starting point for observing quantum effects. For example, in order to apply the necessary and sufficient conditions of the entanglement and spin squeezing [9, 10] one has to know the variance of the CSS. Unlike in case of the shot noise of light, atomic coherent state noise cannot be easily established via independent measurements. It therefore has to be determined

experimentally in each case.

In this paper we report measurements of the orientation, the coherence time, and the number of atoms in a spin ensemble in one selected hyperfine ground state (e.g. the  $F = 4$  states in cesium). This is done by inducing weak transitions among the Zeeman sublevels by radio-frequency magnetic fields. Other similar probing methods have been demonstrated in [11] where microwave magnetic fields on the hyperfine transition are used to characterize the efficiency of optical pumping into e.g. the  $F = 3$ ,  $m_F = 0$  state. Also, fluorescence from atoms excited by the pumping process can give information about the excited spin state which again hints on the ground spin state [12]. In the literature, the spin state of atoms is often modelled by numerical solutions to rate equations. We make a different approach by tailoring simple ad hoc models to describe the main features of the spin state.

The paper is arranged as follows. In section II we describe the ground spin state of our atoms theoretically. This includes an introduction to the notation and the particular physical system used in the experiment II A, deriving equations of motion II B, and modelling the distribution and coherence time of atoms among Zeeman sublevels II C. In the experimental section III we describe the actual setup III A, discuss the conditions for resolving the quadratic Zeeman effect III B, and demonstrate that our models actually describe the experiments III C. Much of the emphasis is put on the quadratic Zeeman effect and the ability to resolve this spectroscopically. However, in some experimental conditions this is not the case and we discuss how we can employ our techniques in a non-resolved regime III D and also in a regime with pulsed lasers IV. In appendix A we review the quadratic

---

\*Electronic address: polzik@nbi.dk

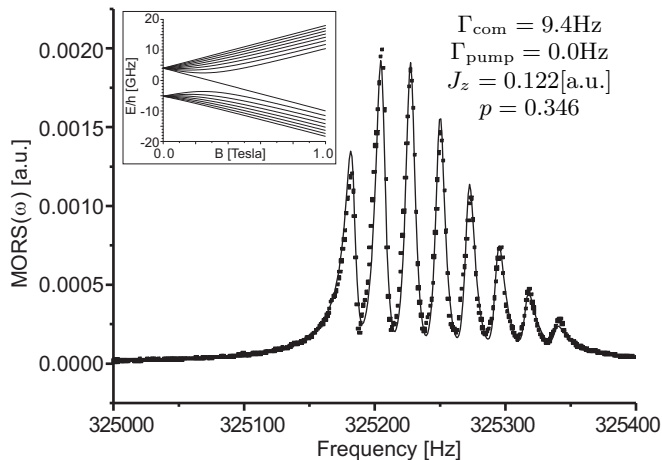


FIG. 1: An experimental spectrum (dots) of magnetic transitions among the nine sublevels of the  $F = 4$  ground state in cesium. An external RF-magnetic field (the frequency of which is shown on the abscissa) modulates the spin state. The recorded response, called the magneto-optical resonance signal (MORS), is shown on the ordinate axis. The solid line is a fit to a model to be developed in section II C, where the parameters and the definition of MORS will also be carefully explained. The many peaks tells us that atoms are distributed among all nine levels resulting in a low orientation  $p = 0.346$ . The line width 9.4 Hz is a direct measure of the decay rate of spin coherence. According to Eq. (A5) the corresponding  $F = 3$  signal is approximately 1 kHz away and does not interfere here. The inset shows the level structure of the ground states of cesium following Eq. (A2). Our experiment is carried out around  $10^{-4}$  T which is far into the linear regime. However, with a sufficiently good resolution the quadratic effect is visible.

Zeeman effect.

## II. THEORETICAL DESCRIPTION

In this section, we introduce the physics and notation which will enable us to understand how magneto-optical resonance can be used to characterize the spin state of an atomic gas sample.

### A. Spin State Evolution in the Process of the Double Magnetic Resonance

Let us consider an ensemble of atoms in a Zeeman multiplet in the ground state of an alkali, in our case this is the  $F = 4$  state in cesium. Applying an external magnetic field, the energy of each magnetic sublevel changes as shown in the inset of Fig. 1. For low fields the splitting between two levels grows linearly with field strength with small quadratic corrections given by  $\nu_{\text{QZ}} = 2\nu_{\text{L}}^2/\nu_{\text{hfs}}$ , where  $\nu_{\text{L}}$  is the Zeeman splitting, or the Larmor frequency, and  $\nu_{\text{hfs}}$  is the hyperfine splitting. This is known

as the quadratic Zeeman effect, for completeness we have summarized the most important results in appendix A.

Applying RF-magnetic fields we can induce transitions between magnetic sublevels. Our spectral resolution is sufficiently high in order to observe the small energy shifts caused by the quadratic Zeeman effect, see Fig. 1. We see eight distinct lines corresponding to transitions between two adjacent levels among the  $2F + 1$  possible levels in the  $F = 4$  state. The connection between the spin state and the spectrum in Fig. 1 will be derived in the following, we will be able to fully characterize the spin state in many situations important for other experiments.

We characterize the state of atoms by the density operator  $\hat{\rho}_{ij}$  given by

$$\hat{\rho}_{ij} = \frac{1}{N} \sum_{k=1}^N \hat{\rho}_{ij}^{(k)} = \frac{1}{N} \sum_{k=1}^N |i\rangle_k \langle j|_k \quad (1)$$

where  $i, j = -F, -F + 1, \dots, F$  parametrizes the magnetic sublevels  $|i\rangle$  or  $|j\rangle$  in Dirac notation, and the sum is done over all individual atoms. With the  $z$ -axis as quantization axis we may express the total macroscopic angular momentum of the atoms in the hyperfine state  $F$  as

$$\begin{aligned} \hat{F}_x &= \frac{1}{2} \{ \hat{F}_+ + \hat{F}_- \} = \\ &= N \sum_{m=-F}^{F-1} \frac{C(F, m)}{2} \{ \hat{\rho}_{m+1, m} + \hat{\rho}_{m, m+1} \} \end{aligned} \quad (2a)$$

$$\begin{aligned} \hat{F}_y &= \frac{1}{2i} ( \hat{F}_+ - \hat{F}_- ) = \\ &= N \sum_{m=-F}^{F-1} \frac{C(F, m)}{2i} \{ \hat{\rho}_{m+1, m} - \hat{\rho}_{m, m+1} \} \end{aligned} \quad (2b)$$

$$\hat{F}_z = N \sum_m m \hat{\rho}_{mm} \quad (2c)$$

where  $C(F, m) = \sqrt{F(F+1) - m(m+1)}$  and  $\hat{F}_{\pm}$  are raising/lowering operators for the spin along  $z$ . Note, if we are interested in calculating the spin components of  $\mathbf{F}$ , it suffices to calculate the diagonal terms and the first off-diagonal terms in the density matrix. This enables us to describe effects like the *orientation* of the spin state, see Sec. II C. In general, to describe aspects of *alignment* we also need second off-diagonal terms. We restrict our description to diagonal and first off-diagonal terms in the following.

The Hamiltonian of spins subject to a magnetic field  $\mathbf{B}$  can be written

$$\hat{H} = g_F \mu_B \mathbf{F} \cdot \mathbf{B} + O(B^2) \quad (3)$$

where the second order correction is described in appendix A. We will partly include this second order correction, since it will prove to be important for the energy levels. We will place a constant bias magnetic field with

strength  $B_{\text{bias}}$  along the  $z$ -axis and apply an RF-magnetic field  $|B_{RF}| \cos(\omega t + \phi)$  along the  $x$ -axis. The Hamiltonian may now be written (for a single atom)

$$\hat{H} = \sum_{m=-F}^F \hbar\omega_m \cdot \hat{\rho}_{mm} + \frac{g_F\mu_B}{4N} \left( \hat{F}_+ B_{RF} e^{-i\omega t} + \hat{F}_- B_{RF}^* e^{i\omega t} \right) \quad (4)$$

where  $B_{RF} = |B_{RF}|e^{-i\phi}$  is the complex amplitude. The first term is primarily  $F_z B_z$ , but we take the second order corrections into account by explicitly stating the energy levels  $\hbar\omega_m$  of the  $m$ 'th sublevel. The second term is  $\hat{F}_x B_x$  originating from the  $x$ -polarized RF-magnetic field which induces transitions between the magnetic sublevels. The rotating wave approximation has been made here. We may wish to write the Hamiltonian entirely in terms of the density operators  $\hat{\rho}_{ij}$ :

$$\hat{H} = \sum_{m=-F}^F \hbar\omega_m \cdot \hat{\rho}_{mm} + \frac{g_F\mu_B}{4} \sum_{m=-F}^{F-1} (C(F, m)\hat{\rho}_{m+1, m} B_{RF} e^{-i\omega t} + \text{h.c.}) \quad (5)$$

The equations of motion are now determined by

$$\frac{\partial \hat{\rho}_{ij}}{\partial t} = \frac{1}{i\hbar} [\hat{\rho}_{ij}, \hat{H}] + \text{decay terms} \quad (6)$$

where the first term is the coherent evolution of the system, and the interaction with the environment will be put in by hand as decay terms.

## B. Solution of equations of motion

We will now solve equations (5) and (6), and to illuminate the method for solving these equations, we will pick out a single example and work it out thoroughly. The time derivative of e.g.  $\hat{\rho}_{12}$  is

$$\begin{aligned} \frac{\partial \hat{\rho}_{12}}{\partial t} &= \frac{1}{i\hbar} [\hat{\rho}_{12}, \hat{H}] - \Gamma/2 \cdot \hat{\rho}_{12} \\ &= -i(\omega_2 - \omega_1)\hat{\rho}_{12} - \Gamma/2 \cdot \hat{\rho}_{12} \\ &\quad + \frac{ig_F\mu_B}{4\hbar} \{ C(F, 1)[\hat{\rho}_{22} - \hat{\rho}_{11}] B_{RF} e^{-i\omega t} \\ &\quad + [C(F, 0)\hat{\rho}_{02} - C(F, 2)\hat{\rho}_{13}] B_{RF}^* e^{i\omega t} \} \end{aligned} \quad (7)$$

where we have just inserted the Hamiltonian (5) into (6) and added the decay term,  $-\Gamma/2 \cdot \hat{\rho}_{12}$ . We will restrict ourselves to a description of spins in the case where  $F_x, F_y \ll F_z$ , i.e. the angle  $\theta$  that the spins deviate from being oriented along the  $z$ -axis is much less than unity. From equations (2a-2c) this can roughly be written as  $\hat{\rho}_{m+1, m} \approx \theta \cdot \hat{\rho}_{m, m}$ , and following the same lines  $\hat{\rho}_{m+2, m} \approx \theta^2 \cdot \hat{\rho}_{m, m}$ . It is then justified to neglect the coherences  $\hat{\rho}_{02}$  and  $\hat{\rho}_{13}$  in the above equation. For brevity we will define  $\omega_{21} = \omega_2 - \omega_1$ , which is the frequency corresponding to the transition from  $m_F = 2$  to  $m_F = 1$ . This frequency is the Larmor frequency and it is fast compared to the inverse time scale for dynamical evolution of the spin state. Since the RF-magnetic field frequency  $\omega$  will be in the vicinity of  $\omega_{21}$  it will be convenient to define the slowly varying operators

$$\hat{\rho}_{ij} = \tilde{\rho}_{ij} e^{-i\omega t} \quad (8)$$

Using this definition, equation (7) will turn into

$$\begin{aligned} \frac{\partial \tilde{\rho}_{12}}{\partial t} &= (i[\omega - \omega_{21}] - \Gamma/2)\tilde{\rho}_{12} \\ &\quad + \frac{ig_F\mu_B}{4\hbar} C(F, 1) B_{RF} [\hat{\rho}_{22} - \hat{\rho}_{11}] \end{aligned} \quad (9)$$

The constant  $\Gamma$  will describe the decay of the *transverse* spin components. We will assume the time scale  $T_2$  for the transverse spin decay is much shorter than the time scale  $T_1$  for the longitudinal spin component (along the  $z$ -axis). Experimentally we typically find  $T_1 \approx 200\text{-}300\text{ms}$  and  $T_2 \leq 40\text{ms}$  and the approximation is justified. Then the operator  $\tilde{\rho}_{12}$  will follow  $(\hat{\rho}_{22} - \hat{\rho}_{11})$  adiabatically which is expressed mathematically by setting  $\partial \tilde{\rho}_{12} / \partial t = 0$  in the above equation. Alternatively, if constant pumping maintains  $F_z$  the small angle condition  $\theta \ll 1$  will ensure constant  $(\hat{\rho}_{22} - \hat{\rho}_{11})$ . Then the above is simply the steady state condition where transients have been damped away. The result for  $\hat{\rho}_{12}$  is then

$$\hat{\rho}_{12} = -\frac{ig_F\mu_B B_{RF} C(F, 1) e^{-i\omega t}}{4\hbar \cdot (i[\omega - \omega_{21}] - \Gamma/2)} [\hat{\rho}_{22} - \hat{\rho}_{11}] \quad (10)$$

This method applies to all density operators  $\hat{\rho}_{m, m+1}$ , and substituting into equations (2a) and (2b) we get

$$\hat{F}_x = \text{Re} \left\{ \frac{ig_F\mu_B B_{RF} N}{4\hbar} \sum_{m=-F}^{F-1} \frac{[F(F+1) - m(m+1)] \cdot e^{i\omega t}}{i(\omega_{m+1, m} - \omega) - \Gamma_{m+1, m}/2} [\hat{\rho}_{m+1, m+1} - \hat{\rho}_{m, m}] \right\} \quad (11a)$$

$$\hat{F}_y = \text{Im} \left\{ \frac{ig_F\mu_B B_{RF} N}{4\hbar} \sum_{m=-F}^{F-1} \frac{[F(F+1) - m(m+1)] \cdot e^{i\omega t}}{i(\omega_{m+1, m} - \omega) - \Gamma_{m+1, m}/2} [\hat{\rho}_{m+1, m+1} - \hat{\rho}_{m, m}] \right\} \quad (11b)$$

These equations can be interpreted as a number ( $2F$ ) of two-level systems that all interact with the driving RF-magnetic field. Two adjacent magnetic sublevels  $m$  and  $m+1$  act as one two-level atom with the usual Lorentzian response (resonance frequency  $\omega_{m+1,m}$  and line width  $\Gamma_{m+1,m}$  FWHM). Each two-level system does not respond with exactly the same weight which is reflected in the factor  $F(F+1) - m(m+1)$ . All the resonances add up coherently to give the overall response of the spin state to the RF-magnetic field. Note, that  $\hat{F}_x$  and  $\hat{F}_y$  oscillate at the driving frequency  $\omega$  and not the “natural” frequencies  $\omega_{m+1,m}$ . This is a steady state behavior, just like the forced harmonic oscillator when transients have been damped. In section IV we will comment on non-steady state behavior of the spin system.

### C. Modeling the spin state

In the previous subsection we derived how the spin  $\mathbf{F}$  responds to an external RF-magnetic field  $\mathbf{B}_{\text{RF}}$ . Our main motivation is to use this knowledge to characterize the spin state, i.e. we wish to apply the field  $\mathbf{B}_{\text{RF}}$  and measure the response  $\hat{F}_x$  or  $\hat{F}_y$  in order to deduce parameters like  $\hat{\rho}_{m,m}$ ,  $\Gamma_{m+1,m}$  and so on. Now, for cesium in the  $F = 4$  hyperfine ground state there are nine populations  $\hat{\rho}_{m,m}$  and eight line widths  $\Gamma_{m+1,m}$  together with the resonance frequencies. To fit an experimentally measured spectrum (see e.g. Fig. 1) to all these parameters will be very hard and in the following we will develop a model to significantly reduce the number of free parameters. We will just tailor a model and the justification for this model will be an experimental test.

Let us consider a case where we wish to orient all atomic spins along the  $z$ -direction, i.e. attempt to put many atoms into the  $m = F$  substate. This can be done experimentally by illuminating the atoms with circularly polarized light, as will be described in the experimental section. It is then convenient to define the orientation  $p$  as an order of merit

$$p = \frac{1}{F} \sum_{-F}^F m \cdot \hat{\rho}_{m,m} = \frac{\hat{F}_z}{NF} \quad (12)$$

Note, that with this definition  $p = 1$  if all atoms are in the extreme  $m = F$  sublevel, and  $p = 0$  for a completely unpolarized sample with  $\hat{\rho}_{m,m} = 1/(2F+1)$  for all  $m$ . We try to let this be the only parameter describing the relationship between the nine populations  $\hat{\rho}_{m,m}$ . With the condition  $\sum \hat{\rho}_{m,m} = 1$  we have thus reduced eight free parameters to a single one.

Now, we describe ensembles of atoms and given  $p$  we will assume that the spin state maximizes the entropy  $S = -\text{Tr}(\hat{\rho} \ln \hat{\rho})$ . To find the individual  $\hat{\rho}_{m,m}$  we use the

method of Lagrange multipliers. We must solve

$$\begin{aligned} \frac{\partial}{\partial \hat{\rho}_{m,m}} \left( S - \alpha \sum \hat{\rho}_{m,m} - \beta \sum m \cdot \hat{\rho}_{m,m} \right) &= 0 \\ \Rightarrow \hat{\rho}_{m,m} &= e^{-1-\alpha} \cdot e^{-\beta \cdot m} \end{aligned} \quad (13)$$

We now just need to adjust  $\alpha$  and  $\beta$  in order that  $\text{Tr}(\hat{\rho}) = 1$  and  $p$  is as desired. Doing this is more or less a computational problem and in principle not difficult. For the physical understanding we just need to remember that we can write  $\hat{\rho}_{m,m} \propto \epsilon^m$  where  $\epsilon = e^{-\beta}$  is a parameter which is a function of  $p$ . This can go directly into equations (11a) and (11b). We stress that the above considerations are meant as an intuitive guideline to understand what is really just an experimentally justified model. This model is only valid in some specific cases, our example with circular polarized pumping light. Our experience tells us that the model works fine for large longitudinal relaxation times  $T_1$  and not too strong influence by the probe laser.

For the eight line widths  $\Gamma_{m+1,m}$  in the case of cesium we will make a model with two free parameters. First, a common line width  $\Gamma_{\text{com}}$  is assigned to all transitions independent of  $m$ . The physical cause for this type of decay could be magnetic field inhomogeneities, collisions, and loss mechanisms common to all atoms. In addition, if we wish to create a well oriented sample with  $m$  approaching  $F$  we will need to illuminate the atoms with resonant circularly polarized light. In our case this is the 894nm  $6S_{1/2}, F = 4$  to  $6P_{1/2}, F' = 4$  line. This light causes excitations from the atomic ground sublevel  $m$  with a rate  $\gamma_m \propto |\langle 4, m, 1, 1 | 4, m+1 \rangle|^2 = (4-m)(5+m)/40$ , where the second term is the square of Clebsch-Gordan coefficients. For a magnetic transition between ground sublevels  $m$  and  $m+1$  the resonant pumping light will contribute to the line broadening proportional to  $\gamma_m + \gamma_{m+1}$ . Thus we define the width  $\Gamma_{\text{pump}}$  caused by the optical pumping process such that

$$\Gamma_{m+1,m} = \Gamma_{\text{com}} + \Gamma_{\text{pump}} \frac{19 - 2m - m^2}{4} \quad (14)$$

where the normalization is such that for the  $m = 3 \rightarrow m = 4$  transition we have  $\Gamma_{4,3} = \Gamma_{\text{com}} + \Gamma_{\text{pump}}$ .

Finally, we must have the resonant frequencies as parameters in our model. We will write this as a central frequency  $\omega_{\text{center}}$  and a splitting  $\omega_{\text{split}}$  such that

$$\omega_{m+1,m} = \omega_{\text{center}} + \omega_{\text{split}} \left( m + \frac{1}{2} \right) \quad (15)$$

Theoretically we should have  $\omega_{\text{split}} = 2\pi \cdot \nu_{\text{QZ}}$  (see equation (A7)) but we keep it as a free parameter since in practice this splitting may differ slightly from the theoretical value because of Stark splittings.

To sum up, a possible description of the ground spin state involves the total spin  $\hat{F}_z$  and the orientation  $p$  together with the line widths  $\Gamma_{\text{com}}$  and  $\Gamma_{\text{pump}}$ , and the frequencies  $\omega_{\text{center}}$  and  $\omega_{\text{split}}$ . An equivalent but computationally easier way to represent  $\hat{F}_z$  and  $p$  is to use the

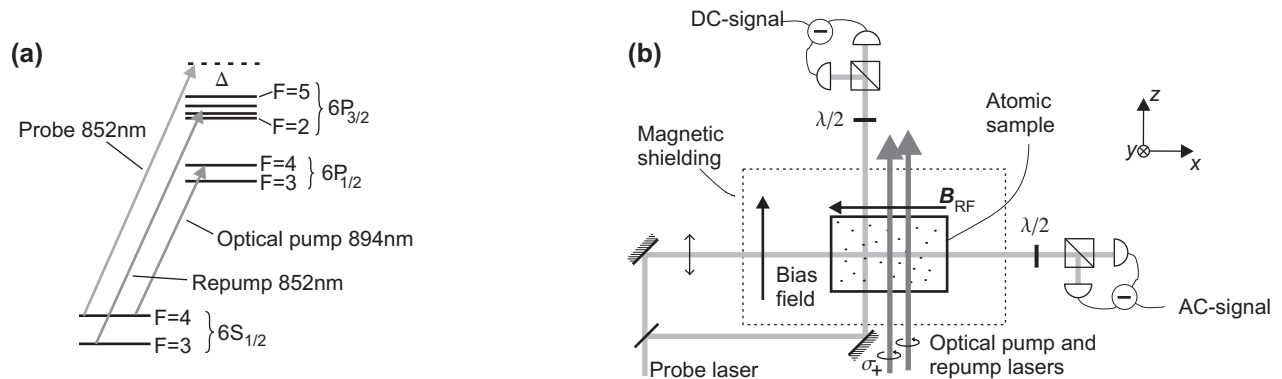


FIG. 2: (a) The lasers used in the experiment together with the level scheme of cesium. The  $F = 4$  ground state is with its nine sublevels of main interest in this experiment. (b) The experimental setup. The atomic ensemble is illuminated with optical pumping and repumping lasers with  $\sigma_+$ -polarized light parallel to a static bias magnetic field. This orients the spins along the  $z$ -axis and gives rise to a 325kHz Larmor precession. An RF-magnetic field perpendicular to the spins induce small spin components in the plane orthogonal to  $z$  which are read out by polarization rotation of a linearly polarized probe laser beam (giving an AC-signal). The spin along  $z$  can also be read out on a probe laser beam (giving a DC-Faraday signal).

number of atoms  $N_4 = N\hat{\rho}_{44}$  of atoms in  $m = 4$  as one parameter and the parameter  $\epsilon$  such that the population  $N_m$  can be expressed as  $N_m = N\hat{\rho}_{m,m} = N_4\epsilon^{(4-m)}$ .

### III. EXPERIMENT

In this experimental section we will first describe the experimental setup in order to understand what is actually measured and how the measurements relate to the equations of section II. Having this in place we comment on the requirements that actually allow us to resolve the individual sublevels as seen in Fig. 1.

#### A. Experimental setup

The experimental setup and the laser level scheme is shown in Fig. 2. Referring to part (a) of the figure, we have a Ti:Sapphire laser probe detuned by  $\Delta \approx 1\text{GHz}$  from the  $6S_{1/2}, F = 4 \rightarrow 6P_{3/2}, F = 5$  transition at 852nm. This laser is sensitive to the state of atoms in the  $F = 4$  ground state and will be used to probe these atoms. To control the state of atoms in the  $F = 4$  ground state we have two home built grating stabilized diode lasers. The *repump laser* is tuned to the  $6S_{1/2}, F = 3 \rightarrow 6P_{3/2}, F = 4$  transition at 852nm. This mainly serves to remove atoms from the otherwise dark  $F = 3$  ground state. The *optical pump laser* tuned to the  $6S_{1/2}, F = 4 \rightarrow 6P_{1/2}, F = 4$  transition at 894nm plays the most important role in distributing atoms among the sublevels of the  $F = 4$  ground state. Note, that atoms in the extreme  $F = 4, m_F = 4$  state will not absorb light from any of the two lasers.

Now turning to Fig. 2b, we place a paraffin coated vapor cell containing cesium inside a shield of  $\mu$ -metal to isolate the atoms from laboratory and Earth magnetic

fields. A static magnetic field of strength approximately 0.9 Gauss is then applied in the  $z$ -direction and the repump and optical pump lasers are illuminating atoms along that direction. The polarization of these lasers can be adjusted, and by choosing circular polarization we can orient the atomic spins along the  $z$ -direction.

The probe laser is split into two beams. One of them is directed along the  $x$ -direction transverse to the atomic magnetization created by the repump and optical pump lasers. This probe laser is linearly polarized along the  $z$ -direction and will undergo polarization rotation proportional to the spin  $\hat{F}_x$  along the  $x$ -axis (see e.g. [8, 13]). By suitable arrangement of a  $\lambda/2$ -plate and a PBS, the difference signal of two photo detectors will be proportional to the polarization rotation (for small angles).

The atomic spins  $\hat{F}_x$  along the  $x$ -axis will have zero mean value unless an RF-magnetic field is applied transversely to the static magnetic field. We apply such a field at frequency  $\omega$  (we shall call this frequency the local oscillator frequency), and the motion of  $\hat{F}_x$  will now be described by equation (11a). We may write the outcoming AC-signal as  $i(t) = \alpha \cdot \hat{F}_x = \alpha \cdot \text{Re}\{A(t)\}$  where  $\alpha$  is a constant depending on beam geometry, laser detuning and intensity [8], and  $A(t)$  reflects the curly bracket of equation (11a). We know from this equation that  $A(t) \equiv A(\omega)e^{i\omega t}$  will possess only a single frequency component, namely the local oscillator frequency  $\omega$  driving the transverse spins  $\hat{F}_x$  and  $\hat{F}_y$  away from zero. The amplitude of this frequency component is experimentally measured by inserting the photo current  $i(t)$  into a lock-in amplifier and decomposing the signal into sine and cosine components:

$$i(t) = \alpha \cdot \text{Re}\{A(\omega)e^{i\omega t}\} \\ = \alpha \cdot (\text{Re}\{A(\omega)\} \cos(\omega t) - \text{Im}\{A(\omega)\} \sin(\omega t)) \quad (16)$$

The lock-amplifier may give the sum of the squared amplitudes of the sine and cosine components which in our

case will be exactly  $\alpha^2|A(\omega)|^2$ . We shall call this signal our *magneto-optical resonance signal* at frequency  $\omega$

(MORS( $\omega$ ) in short). Combining the above with equation (11a) and ignoring irrelevant constants we find

$$\text{MORS}(\omega) = \text{const} \cdot \left| N \sum_{m=-F}^{F-1} \frac{[F(F+1) - m(m+1)]}{i(\omega_{m+1,m} - \omega) - \Gamma_{m+1,m}/2} [\hat{\rho}_{m+1,m+1} - \hat{\rho}_{m,m}] \right|^2 \quad (17)$$

The second part of the probe laser beam in Fig. 2b is linearly polarized and is directed along the static magnetic field direction and will be subject to polarization rotation proportional to the atomic spin  $\hat{F}_z$ . The angle of rotation  $\theta_{\text{DC}}$  (denoted the DC-Faraday rotation angle) can be measured and we have in analogy with (17)

$$\theta_{\text{DC}} = \text{const} \cdot \hat{F}_z = \text{const} \cdot N \sum_{m=-F}^F m \hat{\rho}_{m,m} \quad (18)$$

With the magneto-optical resonance signal, the DC-Faraday rotation angle, and the methods of section II C at hand we will be able to say much about the number of atoms  $N$  of the sample, the populations  $\hat{\rho}_{m,m}$  and the decay rates  $\Gamma_{m+1,m}$  of the coherences  $\hat{\rho}_{m,m+1}$ .

### B. Resolving the different Zeeman lines

To resolve the different Zeeman lines we obviously need  $\Gamma_{m+1,m} \lesssim \omega_{\text{QZ}}$ . There are many contributions to the decay of the transverse coherences, collisions between atoms, collisions with the cell walls, power broadening by laser light, dephasing by magnetic field inhomogeneities.

Atoms are kept in a paraffin coated glass cell which prevents atoms from depolarizing when hitting the walls. This method can increase the coherence time up to roughly 1 second [14]. However, our record is somewhat lower at 50ms.

The probe laser beams give only a marginal contribution to the decay if they are detuned sufficiently far from the resonance or has a low intensity. We estimate the rate  $\Gamma_{\text{ph}}$  at which an atom scatters photons by the two-level atom result (see e.g. [15])

$$\Gamma_{\text{ph}} = \frac{\gamma}{2} \frac{s}{1+s} \approx \frac{3I\lambda^3\gamma^2}{16\pi^2\hbar c\Delta^2} \quad (19)$$

where  $s = \frac{I/I_{\text{sat}}}{1+(2\Delta/\gamma)^2}$  is the saturation parameter.  $I$  is the beam intensity with  $I_{\text{sat}} = 2\pi^2\hbar c\gamma/3\lambda^3$  being the saturation intensity.  $\lambda$  is the optical wave length,  $\gamma$  is the natural line width of the optical transition, and  $\Delta$  is the detuning (assumed much greater than  $\gamma$  in the last step of the equation). In our case we operate at up to  $1\text{mW}/\text{cm}^2$  and the detuning is typically around  $1\text{GHz}$  which contributes the order of  $\Gamma_{\text{ph}} = 100\text{Hz}$  to the decay

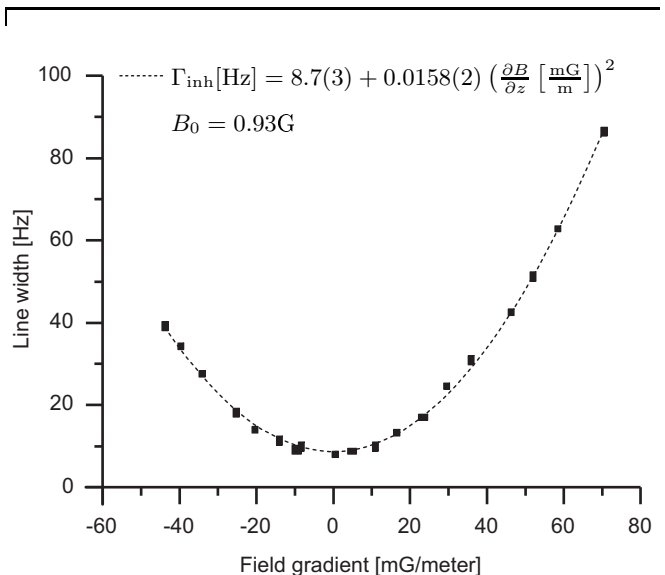


FIG. 3: The measured line width as a function of an applied magnetic field gradient. We confirm the scaling derived in equation (20). The 8.7Hz minimum is set by collisions, power broadening or possible residual inhomogeneities and the additional quadratic part stems from the applied magnetic field inhomogeneity.

rate according to the above estimate. We usually observe a somewhat smaller width which probably can be attributed to the crude two-level atom approximation. Nonetheless, to be able to see the magneto-optical resonance signal a considerably weaker probe can be used and the power broadening can easily be reduced below 1Hz.

The repump laser beam is detuned roughly 9GHz from the  $F = 4$  ground state and thus plays a very minor role even at strong intensities. The optical pump laser is directly on resonance with the  $F = 4$  ground state sublevels and then only a moderate intensity can be allowed if different Zeeman lines should be resolved. The quantitative aspects of the optical pump laser power broadening was discussed in equation (14).

The magnetic field must be homogeneous to a high degree. Since atoms are moving around in the magnetic field, different atoms will experience different magnetic field strengths and hence different Larmor frequencies. To estimate the role of a possible gradient  $\partial B/\partial z$  we use the following simple model (see e.g. [16]). First, divide

the atomic sample into two parts, 1 and 2, along the bias magnetic field direction. If the sample length is  $L$  and the bias field has strength  $B_0$ , the field strength in the two parts will be of order  $B_0 \pm \partial B / \partial z \cdot L$  and the difference in Larmor frequency will be  $(g_F \mu_B / \hbar) \partial B / \partial z \cdot L$  according to (A4). We follow an atom during the time  $T$  it takes for it to decohere. If  $v$  is a typical speed of the atomic motion, the number of visits  $n_1$  in part 1 or  $n_2$  in part 2 will be of order  $Tv/L$ , since each visit has duration  $L/v$ . The difference  $n_1 - n_2$  has mean zero and standard deviation of the order  $\text{std}(n_1 - n_2) = \sqrt{Tv/L}$ . Thus the uncertainty  $\delta\phi$  in the accumulated phase during Larmor precession is

$$\begin{aligned} \delta\phi &\approx \frac{g_F \mu_B}{\hbar} \cdot \frac{\partial B}{\partial z} L \cdot \frac{L}{v} \cdot \text{std}(n_1 - n_2) \approx 1 \\ \Rightarrow \Gamma_{\text{inh}} &\approx \frac{1}{T} \approx \left( \frac{g_F \mu_B}{\hbar} \right)^2 \frac{L^3}{v} \left( \frac{\partial B}{\partial z} \right)^2 \end{aligned} \quad (20)$$

In the first line we set  $\delta\phi$  equal to unity since this is the situation after the time of decoherence  $T$ . We see that the broadening  $\Gamma_{\text{inh}}$  by inhomogeneities scales quadratically with the field gradient. If we take  $g_F \approx 1/4$  (see eq. (A5)),  $L = 0.030\text{m}$ ,  $v = \sqrt{k_B T / m_{\text{Cs}}} = 137\text{m/s}$  at  $T = 300\text{K}$ , we get  $g_F \mu_B / \hbar = 350\text{Hz/mG}$  and expect the broadening to be  $\Gamma_{\text{inh}} = 0.024\text{Hz} \cdot \text{m}^2 / \text{mG}^2 \cdot (\partial B / \partial z)^2$ .

The experimental investigation can be seen in Fig. 3 and we definitely confirm the scaling law predicted above. The numbers match within a factor of two which puts some confidence to our simple model but this is probably also partly luck since we were very crude in the model w.r.t. factors of 2 and  $\pi$ . Comparing the experimental result with the splitting due to the quadratic Zeeman effect (A7) we find for our particular setup that in order to have  $\Gamma_{\text{inh}} < \nu_{\text{QZ}}$  we must have  $1/B \cdot \partial B / \partial z \cdot L < 1.2 \cdot 10^{-3}$ .

### C. Confirming the spin modeling

We will now give experimental support to the theoretical derivations and the modeling of the spin state as described in section II. We first focus on the validity of the simple model introduced in subsection II C, i.e. we test the dependence  $\hat{\rho}_{m,m} \propto \epsilon^m$ , the model for the line widths (14), and the frequency distribution (15).

With the setting as in Fig. 2b we leave the optical pump laser off and vary the polarization of the repump laser. This will create different distributions of  $\hat{\rho}_{m,m}$  and we record the MORS. In Fig. 1 we see an example where all eight lines are clearly visible, the polarization of the repump laser was here quite far away from being purely circular. The dots are experimental points and the solid line is a fit to the model (17) with  $N$ ,  $\epsilon$ ,  $\Gamma_{\text{com}}$ ,  $\omega_{\text{center}}$ , and  $\omega_{\text{split}}$  as free parameters.  $\Gamma_{\text{pump}}$  is set to zero. We see that the solid line matches the experimental points very well. Note, that  $\epsilon$  corresponding to  $p = 0.346$  is the only parameter really describing the relative strength of the

individual peaks, while the other parameters are common to all peaks. The center frequency  $\omega_{\text{center}} \approx 325250\text{Hz}$  is set by the magnetic field (or to be true, this frequency was a quiet place in terms of laser noise for other experiments and thus our detectors was tuned to this frequency). The splitting  $\omega_{\text{split}} = 22\text{Hz}$  is close to the 23Hz expected from Eq. (A7). The small deviation is due to Stark shifts from the laser beams. Finally, we find  $\Gamma_{\text{com}} = 9.4\text{Hz}$  (FWHM). This corresponds to a life time of the spin coherence of 34ms.

The next example is recorded with the repump laser purely circular and optical pump laser still off. The spectrum can be seen in Fig. 4a. Now the spectrum is displaced much more to one side and the fit gives  $p = 0.823$ . This single parameter still seems to describe the shape with good accuracy.

The third example we will show is seen in Fig. 4b. Here the situation is as before but now with a weak optical pump present. We observe an additional broadening of the left most peak by  $\Gamma_{\text{pump}} = 5.5\text{Hz}$  and we also note that the second peak seems much broader (should have an additional broadening by 15.1Hz according to Eq. (14)). Since the fit and the experimental points follow each other very well, we get support for the modeling of  $\Gamma_{\text{pump}}$ . The orientation  $p = 0.967$  shows that we are very close to have all atoms in  $m_F = 4$  with only a moderate amount of optical pumping light.

In the three examples described above we also get a fit for the number of atoms  $N$  on a relative scale (the constant in front of Eq. (17) depends on many experimental parameters so we do not wish to calculate it in absolute units). Multiplying this  $N$  with the fitted orientation  $p$  gives the total spin  $J_z$  (on a relative scale). Now, the DC-Faraday rotation signal  $\theta_{\text{DC}}$  (see (18)) gives an independent measure of  $J_z$  and we may compare the fitted  $J_z$  with  $\theta_{\text{DC}}$  to get another consistency check on the model. This is shown in Fig. 5a where we plot the fitted  $J_z$  as a function of  $\theta_{\text{DC}}$ . The lowest points are taken with the repump laser only and varying repump polarization. The upper eight points are taken with purely circular optical pump of increasing intensity in addition to a purely circular repump laser. We see a very nice agreement between the fitted and the directly measured values giving strong support to both the derivations leading to Eq. (17) and the modeling of the spin state described in subsection II C.

### D. Unresolved lines

The spectra shown so far have been more or less well resolved which enabled us to directly determine the orientation  $p$ . Now, how much information can we extract if the line widths are much broader than the quadratic Zeeman splitting  $\omega_{\text{split}}$ ?

First, assume that all atoms are subject to decoherence with the same rate described by  $\Gamma_{\text{com}} \gg \omega_{\text{split}}$  and decay from pumping light is a small contribution  $\Gamma_{\text{pump}} \approx 0$ .

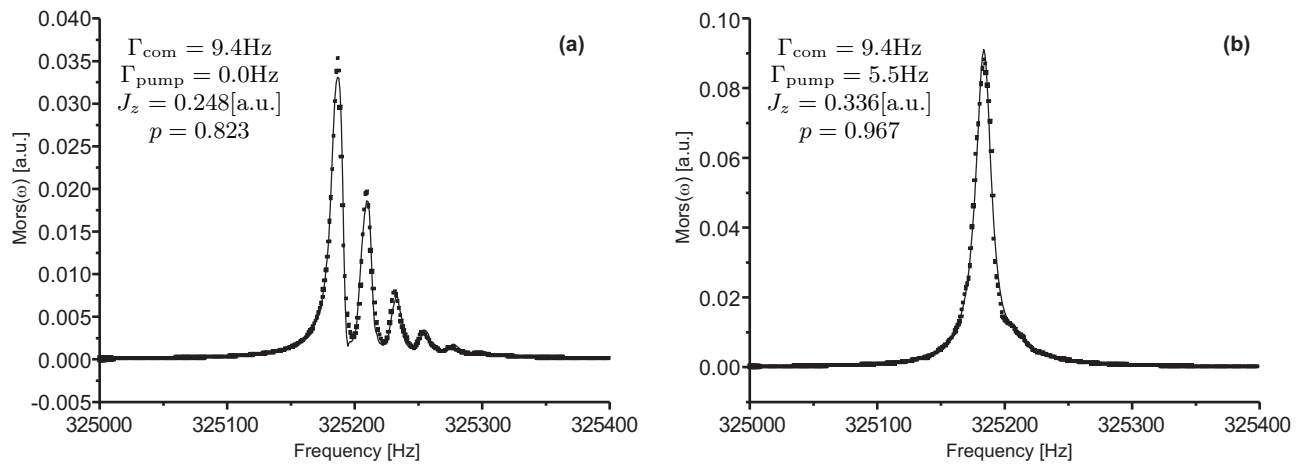


FIG. 4: Two examples of experimental (dots) and fitted (solid line) traces. The left graph was obtained with pure  $\sigma$ -polarized repump laser and no optical pumping. On the right graph a small amount of optical pumping light is added giving rise to a non-zero  $\Gamma_{\text{pump}}$ . Here one can, on careful inspection, observe that the two leftmost peaks have different widths. Note also, that the height has grown by a factor of three compared to the graph on the left.

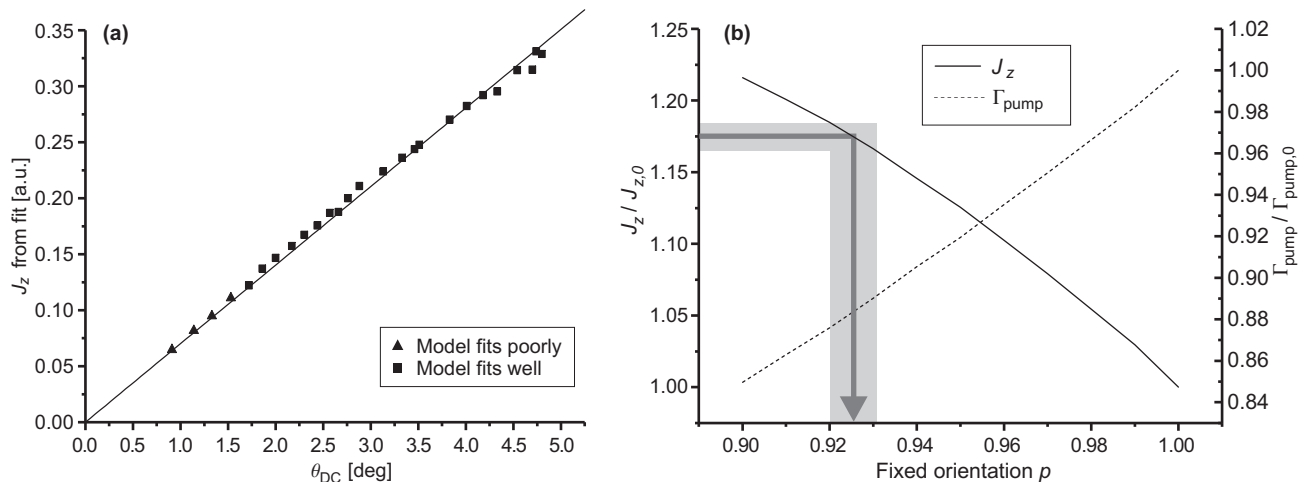


FIG. 5: (a) Consistency check of the models. Fits to different spectra give an estimate of  $J_z$ . This can be compared directly to the independently measured DC-Faraday rotation signal  $\theta_{\text{DC}}$  which is proportional to  $J_z$ . We indeed observe a straight line through the origin. Note, the model description  $\hat{\rho}_{m,m} \propto \epsilon^m$  proved to be less accurate for the lowest four points, but by coincidence the points still fit well. (b) The interdependence of  $p$ ,  $J_z$  and  $\Gamma_{\text{pump}}$  in the limit where  $\Gamma_{\text{pump}}$  dominates both the common width  $\Gamma_{\text{com}}$  and the quadratic Zeeman splitting  $\omega_{\text{split}}$ . Different choices of fitting parameters will lead to a satisfactory fit and additional information is needed to place precise bounds on  $p$ . If for example  $J_z$  is measured independently with an accuracy of 2% the orientation can be defined within 1% in the example shown.

Then Eq. (17) reduces to

$$\text{MORS}(\omega) = \text{const} \cdot \left| 2N \frac{\sum m \hat{\rho}_{m,m}}{i(\omega_0 - \omega) + \Gamma_{\text{com}}} \right|^2 \propto |J_z|^2 \quad (21)$$

We see that in this case the spectrum will be a single Lorentzian the size of which is only depending on  $J_z$ . In this case the independent measure from the DC-Faraday signal would only contribute exactly the same information and we will not be able to deduce the orientation  $p$ .

On the other hand, if  $\Gamma_{\text{pump}}$  dominates  $\Gamma_{\text{com}}$  and  $\omega_{\text{split}}$  we will get a signal that depends on the internal

atomic spin state. To examine this approximation we set  $\Gamma_{\text{com}} = \omega_{\text{split}} = 0$  and try to fit the rest of the parameters to a spectrum which is a perfect Lorentzian. The correct fitting parameters of course have  $p = 1$  and  $\Gamma_{\text{pump}}$  equal to the Lorentzian width but in practical life other sets of parameters will also fit the spectrum to some extent. We find that orientations in the range  $p = 0.9$  to  $p = 1$  result in an agreement one would find reasonable if the spectrum was an experimental trace. By fixing  $p$  to a value in this range, the values given from the fit of  $J_z$  and  $\Gamma_{\text{opt}}$  are shown in Fig. 5b. We see that if we can estimate one of the parameters  $J_z$  or  $\Gamma_{\text{opt}}$  independently we should be able to calculate the orientation  $p$ .



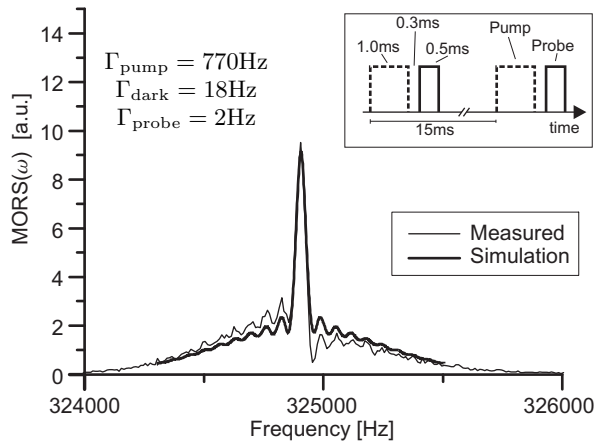


FIG. 6: An example of the magneto-optical resonance signal in a pulsed regime. The spin state is close to the maximal state with  $m_F = 4$  as assumed in the text. Note the ripples which have frequency spacing  $(15\text{ms})^{-1}$ . The decay rate  $\Gamma$  takes different values during one measurement cycle depending on which lasers are on. The timing of laser pulses is shown in the inset and the corresponding decay rates shown on the left part of the figure.

For instance, a measurement of  $J_z$  to an accuracy of 2% will fix the orientation  $p$  to 1%. One only needs to have one fix point, e.g. if one knows that we have  $p = 1$  perfectly in one case, or if one can reduce  $\Gamma_{\text{pump}}$  to the point where the spectral lines become resolved and a calibration like Fig. 5 can be performed. Experimentally we have seen orientations better than  $p = 0.98$  for atomic densities around  $10^{11}\text{cm}^{-3}$ . The optical pumping laser at the 894nm  $D1$ -line is essential to this achievement. We have tried to optically pump on the  $D2$ -line with somewhat lower orientation as a result (a little above  $p = 0.9$ ). A possible explanation is that the rescattered light on the  $F = 4, m_F = 4 \rightarrow F = 5, m_F = 5$  transition from one atom affects the state of other atoms. Indeed, according to [17], even with a dark state when using 894nm pumping light one would expect problems with densities higher than  $\rho_C = (\sigma R)^{-1}$  because radiation will be trapped inside the sample. Here  $\sigma$  is the cross section for light absorption and  $R$  is the extent of the gas sample. Our atomic sample is Doppler broadened with the width  $\delta\nu_D = 378\text{MHz}$ . With a natural line width of the 894nm  $D1$ -transition of  $\gamma = 4.6\text{MHz}$  and a sample extent of  $R = 3\text{cm}$  we estimate the critical density  $\rho_C$  to be roughly  $\rho_C \approx [\lambda^2/2\pi \cdot \gamma/\delta\nu_D \cdot R]^{-1} = 2 \cdot 10^{11}\text{cm}^{-3}$ . We see that we are in the regime where radiation trapping may be a limiting factor, but the experiments tell us that the limitations are still small.

#### IV. PULSED EXPERIMENTS

All previous derivations and measurements have been carried out in cw settings, i.e. Eqs. (11a) and (11b) assume constant values of frequency  $\omega$  and decay rates

$\Gamma_{m+1,m}$ . This is indeed valid if lasers are running cw and if we scan the frequency  $\omega$  slowly enough. But some experiments must be carried out in a setting with pulsed lasers, e.g. one might wish to prepare the spin state in the maximally oriented state  $F = 4, m_F = 4$  by illuminating atoms by a pulse of resonant, circularly polarized laser light. Such state preparation has been used, e.g. for creation of entanglement between two samples of cesium atoms [6]. For the magneto-optical resonance method to be useful in such experiments it must be utilized in the correct experimental conditions which now means time varying decay rates  $\Gamma_{m+1,m}$ . In this section we outline the extensions into the pulsed regimes and discuss the applicability of the magneto-optical resonance method for characterization of spin states under these circumstances.

We assume for simplicity that atoms are pumped to  $m_F = 4$  to an extent that we only need to consider transitions between  $m_F = 3$  and  $m_F = 4$ . The extension to all levels should be straightforward (but cumbersome). For these two levels we may write Eq. (9) as

$$\frac{\partial \tilde{\rho}_{34}}{\partial t} = (i\Delta - \Gamma/2)\tilde{\rho}_{34} + i\chi[\hat{\rho}_{44} - \hat{\rho}_{33}] \quad (22)$$

where  $\Delta = \omega - \omega_{43}$  and  $\chi = g_F\mu_B B_{RF}C(F, 3)/4\hbar$ . We assume as in section II B that the populations  $\hat{\rho}_{44}$  and  $\hat{\rho}_{33}$  can be treated as constants corresponding to small angle deviations from the  $z$ -axis. Then the solution of the above equation is straightforward

$$\tilde{\rho}_{34}(t) = \tilde{\rho}_{34}(0)e^{(i\Delta - \Gamma/2)t} - \frac{i\chi}{i\Delta - \Gamma/2}[\hat{\rho}_{44} - \hat{\rho}_{33}] \left(1 - e^{(i\Delta - \Gamma/2)t}\right) \quad (23)$$

This solution starts out with  $\tilde{\rho}_{34}(0)$  at  $t = 0$  and makes a damped oscillation toward the steady state value  $-i\chi[\hat{\rho}_{44} - \hat{\rho}_{33}]/(i\Delta - \Gamma/2)$ . Note, this steady state value is exactly the result in (10), and it is reached in a time  $\approx \Gamma^{-1}$ . With the solution of  $\tilde{\rho}_{34}$  we can continue to find the actual spin, e.g.  $\hat{F}_x$  given by (2a) and predict the results of a measurement.

Experimentally, we set up pumping lasers and a probe laser measuring the transverse spin state as in Fig. 2b. The lasers are turned on and off with acousto- and electro-optical modulators. The decay rate in the absence of lasers is denoted  $\Gamma_{\text{dark}}$  which is typically small. When the probe laser is on an additional broadening of  $\Gamma_{\text{probe}}$  is present leading to a total decay rate of  $\Gamma_{\text{probe}} + \Gamma_{\text{dark}}$ . During the optical pumping pulse the atoms are typically subject to a high decay rate given in total by  $\Gamma_{\text{pump}} + \Gamma_{\text{dark}}$ . The probe laser is typically turned on shortly after the optical pumping has been turned off and is maintained for a time shorter than the decay time  $(\Gamma_{\text{probe}} + \Gamma_{\text{dark}})^{-1}$ . We are thus in the transient regime of Eq. (23) and given the frequency  $\omega$  of the driving RF-magnetic field we cannot obtain a simple estimate of the amplitude of the response at that frequency as in (17). Instead we have time varying quadrature components of the measured AC-signal and we simply average these over

time in the presence of the probe laser. From the perspective of modeling we need to evolve  $\hat{\rho}_{34}$  according to (23) with the relevant decay rates and integrate the result over the time of the probe laser pulse.

An example of an experimental trace with corresponding numerical modeling is shown in Fig. 6. The inset shows the pulse sequence of lasers with a total period of 15ms. The repump and optical pump lasers are turned on for 1.0ms with a high power making a power broadening  $\Gamma_{\text{pump}} = 770 \pm 30\text{Hz}$ . After a 0.3ms period with lasers off the probe laser is fired for a 0.5ms period giving rise to a small power broadening  $\Gamma_{\text{probe}} \approx 2\text{Hz}$  in addition to the background value around  $\Gamma_{\text{dark}} \approx 18\text{Hz}$ . These decay rates are estimated from cw experiments carried out with the same laser powers. The experimental trace matches quite well the calculated spectrum in the sense that the general trend with a central peak and some broader background structure is present. Also, the 15ms period together with the (rotating frame) oscillation at frequency  $\Delta$  introduces ripples in both the experimental and calculated traces with spacing  $(15\text{ms})^{-1} = 67\text{Hz}$ . However, there is some asymmetry in the experimental trace which naturally is not present in the modeling. This asymmetry could be an effect of non-perfect orientation or maybe an effect of the frequency scan being a little too fast. But this is a minor detail to the general impression that the modeling is doing quite well.

We have tried to vary the duration of the pump pulse, the duration of the probe pulse, and the value of  $\Gamma_{\text{pump}}$ . In all cases we maintain the agreement between measured and calculated spectra as demonstrated for the single example in Fig. 6. If  $\Gamma_{\text{pump}}$  is strong, the magneto-optical resonance signal is essentially a broad feature the structure of which in principle can be calculated. But varying the total number of atoms we have seen experimentally that a simple relation like  $J_z \propto \sqrt{\text{area} \cdot \text{width}}$  practically holds very well where  $J_z$  is measured by a DC-Faraday rotation signal (18) and the area and width refer to the pulsed spectrum. This relation is exact in the cw case for  $p = 1$  but is apparently useful in some cases for the pulsed spectrum. This is an advantage since we in these cases need not perform the more cumbersome modeling suggested by (23).

## V. CONCLUSION

We have studied the magneto-optical resonance for cesium in a vapor cell as a method for characterization of the quantum spin state of the atomic vapor. We have optically pumped the atoms to various distributions among the Zeeman sublevels and exploited the magneto-optical resonance signal, in particular the quadratic Zeeman effect, to characterize these distributions and the decay rate of coherences among the levels.

The theoretical description relies on well known techniques combined with ad hoc tailored models for our particular needs. Specially useful has been the relation

$\hat{\rho}_{m,m} \propto \epsilon^m$  which just happened to be a sufficient model in many of our cases. Our experiments agree very well with the models in the cw case and demonstrate that signals obtained in the pulsed regime are useful and well understood. Our approach with the quadratic Zeeman effect is particularly well suited for characterization of the ground spin state within a hyperfine multiplet. Given the off-resonant laser probe with low photon scattering rate we obtain the required high resolution. The methods could be extended to the microwave region and cover transitions between different hyperfine levels similar to the approach in [11]. For excited spin state characterization the fast spontaneous decay rules out high resolution methods. In this case scattered photons from the pumping process may provide useful information [12].

We have been able to create the coherent spin state to a high degree of accuracy (better than 98%) which is a very good starting point for studies of quantum effects in our spin ensemble. One limitation of our procedure is the fact that high orientations and high pumping rates decrease the possible resolution as discussed in section III D. Thus it takes some effort and experimental stability to see the difference between a 98% and a 100% polarized sample. Also, a pulsed laser setup complicates the conclusions but valuable information can still be extracted. The use of 894nm pumping light on the  $D1$ -transition turns the  $F = 4$ ,  $m_F = 4$  state into a dark state which has proved to be essential to obtain high degrees of orientation.

The reliable method for characterization of a coherent spin state of atoms in a paraffin coated vapor cell described above provides the basis for implementation of various entanglement and quantum communication protocols utilizing collective atomic spin states.

## Acknowledgments

This work was funded by the Danish National Research Foundation and the EU grants CAUAC and QUICOV.

## APPENDIX A: THE QUADRATIC ZEEMAN EFFECT

The quadratic Zeeman effect is well understood [18], we will just outline the important results for completeness of this paper. An alkaline atom in an external magnetic field  $\mathbf{B}$  is described by the Hamiltonian

$$\hat{H} = ha\mathbf{I} \cdot \mathbf{J} - \frac{\mu_J}{J}\mathbf{J} \cdot \mathbf{B} - \frac{\mu_I}{I}\mathbf{I} \cdot \mathbf{B} \quad (\text{A1})$$

where  $\mathbf{J}$  describes the angular momentum of the outermost electron,  $\mathbf{I}$  is the nuclear spin,  $a$  describes the strength of the magnetic dipole interaction between the electronic and nuclear spin, and  $h$  is Planck's constant. The magnetic moment of the electron (for an  $s$ -electron with  $L = 0$ ) is  $\mu_J = -1.0011596521869(41)\mu_B$ . The value for the nuclear moment in cesium is  $\mu_I =$

2.582025(4) $\mu_N$ . Thus, the last term in (A1) always gives a minor correction compared to the second term, but the relative strength between the first and second terms depends on the magnetic field  $\mathbf{B}$ .

The exact solution for the energy  $E$  to the above Hamiltonian is

$$E_{F,m} = -\frac{h\nu_{\text{hfs}}}{2(2I+1)} - \frac{\mu_I}{I}Bm \pm \frac{h\nu_{\text{hfs}}}{2}\sqrt{1 + \frac{4m}{2I+1}x + x^2} \quad (\text{A2})$$

where  $\pm$  is used for  $F = I \pm 1/2$ ,  $m$  is the magnetic quantum number (quantized along the direction of the magnetic field),  $B = |\mathbf{B}|$ , and the hyperfine splitting  $\nu_{\text{hfs}}$  relates to  $a$  by  $h\nu_{\text{hfs}} = \frac{ha}{2}(2I+1)$ . The parameter  $x$  describes the relative strength between the Zeeman effect and the hyperfine splitting:

$$x = \frac{(-\mu_J/J + \mu_I/I)B}{h\nu_{\text{hfs}}} \quad (\text{A3})$$

For weak fields  $m$  describes the projection of the total angular momentum  $\mathbf{F} = \mathbf{I} + \mathbf{J}$ . The energy levels (A2) can be seen in the inset of Fig. 1 as a function of the strength of the magnetic field. We see that for small field strengths or very strong fields, the energy depends linearly on  $B$ . In the intermediate region the situation is quite non-linear. Our experiment is performed in the weak field regime with  $x \approx 3 \cdot 10^{-4}$ . Here a linear approximation is very good, but it is important to calculate also the second order contribution.

We study the magnetic sublevels by inducing magnetic transitions with  $\Delta m = \pm 1$ . Thus, it will be interesting to calculate the separation of adjacent sublevels. We start out by expanding (A2) to first order in the magnetic field strength  $B$  (leaving out the constant shift independent of  $B$ ). With the standard convention

$$E_{F,m}^{(1)} = g_F \mu_B B m \quad (\text{A4})$$

we get for cesium with nuclear spin  $I = 7/2$

$$g_F = \frac{1}{\mu_B} \left( -\frac{\mu_I}{I} \pm \frac{-\mu_J/J + \mu_I/I}{2I+1} \right) \quad (\text{A5})$$

$$= \begin{cases} 0.250390 & \text{for } F = 4 \\ -0.251194 & \text{for } F = 3 \end{cases}$$

These two numbers differ in magnitude by approximately 0.3%. Thus, in the lower linear regime of the inset of Fig. 1 we have a slightly higher separation between levels for the case of  $F = 3$  than  $F = 4$ .

To calculate the quadratic Zeeman shift, it will suffice to do the approximation  $\mu_I = 0$ . In this case we may write the first order expansion of (A2) as  $h\nu_L \equiv E_{m+1} - E_m = \frac{-\mu_J/J}{2I+1} \cdot B$ , and we then easily derive to second order

$$\frac{E_{m+1} - E_m}{h} = \nu_L \left( 1 - \frac{\nu_L}{\nu_{\text{hfs}}} (2m+1) \right) \quad (\text{A6})$$

This equation describes the transition frequency between the  $m$ 'th and the  $(m+1)$ 'th level. The separation  $\nu_{\text{QZ}}$  caused by the quadratic Zeeman effect between two *lines* in e.g. Fig. 1 will thus be

$$\nu_{\text{QZ}} = \frac{2\nu_L^2}{\nu_{\text{hfs}}} \quad (\text{A7})$$

All our experiments reported in this paper will have  $\nu_L$  in the vicinity of 325kHz corresponding to a magnetic field of a little less than 1 Gauss. With the cesium hyperfine splitting being  $\nu_{\text{hfs}} = 9.1926\text{GHz}$  we get a quadratic Zeeman splitting of 23Hz.

- 
- [1] E. B. Alexandrov, M. V. Balabas, A. S. Pazgalev, A. K. Verchovski, and N. N. Yakobson, *Laser Physics* **6**, 244 (1996).
- [2] C. Salomon *et. al.*, *AIP Conf. Proc.* **551**, 23 (2001).
- [3] D. F. Phillips, A. Fleischhauer, A. Mair, R. L. Walsworth, and M. D. Lukin, *Phys. Rev. Lett.* **86**, 783 (2001).
- [4] C. Liu, Z. Dutton, C. H. Behroozi, and L. V. Hau, *Nature* **409**, 490 (2001).
- [5] A. Kuzmich, L. Mandel, and N. P. Bigelow, *Phys. Rev. Lett.* **85**, 1594 (2000).
- [6] B. Julsgaard, A. Kozhekin, and E. S. Polzik, *Nature* **413**, 400 (2001).
- [7] C. Schori, B. Julsgaard, J. L. Sørensen, and E. S. Polzik, *Phys. Rev. Lett.* **89**, 057903 (2001).
- [8] B. Julsgaard, C. Schori, J. L. Sørensen, and E. S. Polzik, To appear in *Quantum Information & Computation*, special issue (2003).
- [9] L.-M. Duan, G. Giedke, J. I. Cirac, and P. Zoller, *Phys. Rev. Lett.* **84**, 2722 (2000).
- [10] D. J. Wineland, J. J. Bollinger, W. M. Itano, F. L. Moore, and D. J. Heinzen, *Phys. Rev. A* **46**, R6797 (1992).
- [11] G. Avila, V. Giordano, V. Candelier, E. de Clercq, G. Theobald, and P. Cerez, *Phys. Rev. A* **36**, 3719 (1987).
- [12] A. Fischer and I. V. Hertel, *Z. Phys. A* **304**, 103 (1982).
- [13] W. Happer and B. S. Mathur, *Phys. Rev. Lett.* **18**, 577 (1967).
- [14] M. A. Bouchiat and J. Brossel, *Phys. Rev.* **147**, 41 (1966).
- [15] H. J. Metcalf and P. van der Straten, *Laser Cooling and Trapping* (Springer, New York, 1999).
- [16] D. Kleppner, N. F. Ramsey, and H. M. Goldenberg, *Phys. Rev.* **126**, 603 (1962).
- [17] D. Tupa and L. W. Anderson, *Phys. Rev. A* **36**, 2142 (1987).
- [18] N. F. Ramsey, *Molecular Beams* (Oxford University

Press, Amen House, London EC4, 1956).